

# Generating stable molecules using imitation and reinforcement learning

Søren Ager Meldgaard,<sup>1</sup> Jonas Köhler,<sup>2</sup> Henrik Lund Mortensen,<sup>1</sup> Mads-Peter V. Christiansen,<sup>1</sup> Frank Noé,<sup>2,3,4</sup> and Bjørk Hammer<sup>1</sup>

<sup>1</sup>*InterCat and Department of Physics and Astronomy, Aarhus University, Denmark.*

<sup>2</sup>*Freie Universität Berlin, Department of Mathematics and Computer Science, Berlin, Germany*

<sup>3</sup>*Freie Universität Berlin, Department of Physics, Berlin, Germany*

<sup>4</sup>*Rice University, Department of Chemistry, Houston, TX, USA*

(Dated: 13 July 2021)

Chemical space is routinely explored by machine learning methods to discover interesting molecules, before time-consuming experimental synthesizing is attempted. However, these methods often rely on a graph representation, ignoring 3D information necessary for determining the stability of the molecules. We propose a reinforcement learning approach for generating molecules in cartesian coordinates allowing for quantum chemical prediction of the stability. To improve sample-efficiency we learn basic chemical rules from imitation learning on the GDB-11 database to create an initial model applicable for all stoichiometries. We then deploy multiple copies of the model conditioned on a specific stoichiometry in a reinforcement learning setting. The models correctly identify low energy molecules in the database and produce novel isomers not found in the training set. Finally, we apply the model to larger molecules to show how reinforcement learning further refines the imitation learning model in domains far from the training data.

## I. INTRODUCTION

Discovering novel molecules or materials with desirable properties is a challenging task because of the immense size of chemical compound space. Further complicating the process is the costly and time-consuming process of synthesizing and testing proposed structures. Whereas this procedure historically was driven by a trial-and-error process, the advance of computational quantum chemical methods allows for initial screening to select promising molecules for experimental testing. While the computational resource growth provided a significant speed-up in processing molecules an exhaustive search of molecular compound space is still infeasible. Instead an automated search for interesting candidates is desired. Examples of such search methods include evolutionary algorithms<sup>1,2</sup>, basin-hopping<sup>3</sup> and particle swarm optimization<sup>4</sup>. More recently, machine learning (ML) enhanced versions of aforementioned methods<sup>5-7</sup> and regression methods facilitating speed-up of virtual screening<sup>8,9</sup> has gained considerable interest by making researchers able to quickly identify attractive candidates for experimental testing. An added benefit of virtual screening is the creation of numerous databases containing structures with computed chemical and physical properties<sup>10-14</sup> leading to generative models for discovery of novel molecules and materials<sup>15-26</sup>. Unlike virtual screening where candidates are selected among the structures in the database, generative models have shown a remarkable ability to leverage the database to produce new structures with desirable properties. A notable limitation is a large database and no feedback-loop to improve the generated molecules beyond what is learned from the database. To remedy this, reinforcement learning (RL) methods have started to become a competitive alternative<sup>27-33</sup> to methods relying on existing databases. RL involves a model that produces molecules and obtains properties

for these molecules, by some external means other than a database. This provides the basis for the model to learn from the molecules it produces. Whereas generative models rely on databases for pretraining, RL is usually done without any prior knowledge leading to initial inefficiency as basic chemical and physical rules are learned. Instead a reward must be defined though, so it requires a setting where a meaningful reward function is available, such as an energy or other things to be optimized. In this work we built upon a previous reinforcement learning algorithm called Atomistic Structure Learning Algorithm (ASLA)<sup>34</sup> by incorporating databases into molecular RL to improve sample efficiency while simultaneously allowing the ML model to learn beyond the knowledge contained in the database. First, a general purpose model is trained using a database to create a model applicable for all stoichiometries. Then, a copy of the general purpose model is created for each stoichiometry of interest. These models are then further refined in a RL setting in a search for low energy isomers for the given stoichiometry. Specifically, we utilize a very small subset of the GDB-11<sup>35</sup> database that consists of small organic molecules satisfying simple chemical stability rules and contains up to 11 atoms of C, N, O and F. We demonstrate that our RL model is able to both replicate structures in the database as well as producing novel low energy structures. By focusing on low energy structures, we believe we avoid the general pitfall of generative models that may produce a large degree of unsynthesizable molecules, as e.g. shown in the work of Gao and Connor<sup>36</sup>. Unlike previous approaches using SMILES<sup>37</sup> or graphs, we operate directly in cartesian coordinates thus allowing for optimization of the potential energy hence easily biasing the search towards thermodynamically stable structures. To improve sample-efficiency we take a model-based approach where, similar to Ref. 38, the potential energy surface is modeled by a

neural network allowing for approximate but cheap optimization. Finally, we introduce an architecture based on SchNet<sup>39</sup> with a self-attention mechanism<sup>40</sup> allowing the RL model to account for long-range effects. The paper is constructed as follows: first the RL theory is outlined, followed by a description of the neural network architecture. Then the database pretraining and RL phase are described before demonstrating the method on a subset of GDB-11. Finally, we apply the method to larger molecules outside the training distribution.

## II. THEORY

The objective of RL is to solve a decision problem, i.e. formulate a program that given an input can decide on the optimal action. Specifically, we refer to this program as an agent which is given a state,  $s$ , and must decide on an action,  $a$ . In the general case the decision process involves multiple steps indexed with the subscript  $t$  while  $T$  is used for the final step. In order to solve the problem the agent must devise a policy,  $\pi$ , which is a probability distribution over the possible actions in a given state. The optimal policy is the policy which maximizes the sum of rewards, where  $r(s)$  is the reward given in state  $s$ . The states, actions and rewards are user-specified and describes the problem to be solved. Following Ref. 33, the state space is defined as all (possibly partial) molecules along with a bag of atoms not yet attached to the molecule. For the reward we seek to minimize the potential energy, i.e. we set intermediate rewards to zero and assign a final reward based on the potential energy of the molecule.

$$r(s_t) = \begin{cases} \max\left(\frac{E_{\text{ref}} - E(s_T)}{\Delta E} + 1, 0\right), & \text{if } t = T \\ 0, & \text{else} \end{cases} \quad (1)$$

Here  $E_{\text{ref}}$  is the lowest energy observed and  $\Delta E = 10\text{eV}$  is the energy span from  $E_{\text{ref}}$  where energy differences are resolved. Note that  $E_{\text{ref}} \leq E(s_T)$  meaning that  $0 \leq r(s_t) \leq 1$ . We scale the reward to stabilize the training as energies of produced structures may fluctuate substantially during the RL phase. To maximize the expected sum of rewards we define the  $Q$ -value,

$$Q_\pi(s, a) = \mathbb{E}_\pi \left[ \sum_{k=t+1}^T r(s_k) \mid s_t = s, a_t = a \right] \\ = \mathbb{E}_\pi [r(s_T) \mid s_t = s, a_t = a], \quad (2)$$

i.e. the expected final reward when taking action  $a$  in state  $s$  and then following policy  $\pi$ . The goal of the agent is to infer the optimal  $Q$ -value function

$$Q_*(s, a) = \max_\pi Q_\pi(s, a) \quad \forall s, a, \quad (3)$$

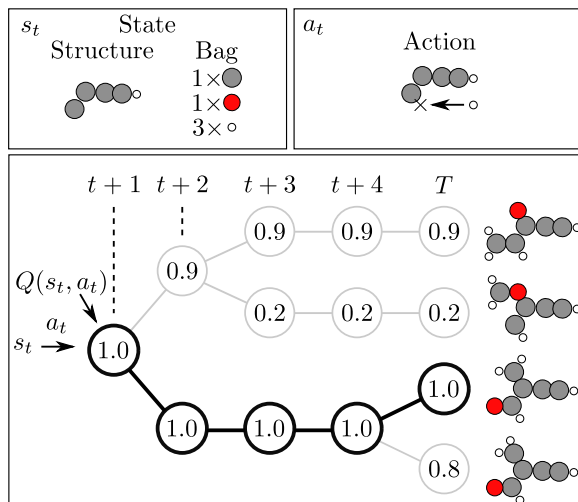


FIG. 1. Given a state,  $s_t$  and an action  $a_t$ , the target  $Q$ -value is calculated by computing the energy of finished structures involving the state-action pair. In the above case a hydrogen atom is placed, which has led to four different structures. The  $Q$ -value is updated towards the reward for the lowest energy structure built.

thereby enabling the agent to perform the best action in every state. To improve the  $Q$ -value function we parameterize it by a neural network and update it as the agent collects new experience. Specifically, we evaluate the  $Q$ -values on a voxelated grid, which allows us to update the  $Q$ -value towards the highest final reward observed by the agent for a specific state-action pair (Fig. 1), which for a deterministic problem puts a lower bound on the optimal  $Q$ -value<sup>41</sup>. Additionally, this discretization allows for easy inference of the optimal atom placement by simply finding the voxel which maximizes the  $Q$ -value.

## III. ARCHITECTURE

The state representation is utilized for calculating the energy of a structure as well as a state value which is used for calculating the  $Q$ -value, but is independent of the specific action. For improved data efficiency the state and action representation must satisfy symmetries in the Hamiltonian, i.e. translation, rotation and mirroring of the molecule as well as permutation of identical atoms. To incorporate these properties in the state representation we utilize pairwise distances (Fig. 2a, **D**), expanded in a Gaussian basis

$$\mathbf{D}_{ijk} = e^{-\gamma(r_{ij} - \mu_k)^2} f_c(r_{ij}) \quad (4)$$

where  $\gamma = 1\text{\AA}^{-2}$  and  $r_{ij}$  is the distance between atom  $i$  and  $j$ . For  $\mu_k$ , we choose 20 values uniformly between 0 and a cutoff-radius  $r_c = 5\text{\AA}$ . The cutoff function

$$f_c(r) = \begin{cases} \frac{1}{2} \left( \cos\left(\frac{\pi r}{r_c}\right) + 1 \right), & \text{if } r \leq r_c \\ 0, & \text{else} \end{cases} \quad (5)$$

emphasizes the importance of the local neighborhood by decaying  $\mathbf{D}_{ijk}$  as a function of  $r_{ij}$  and ensures a smooth transition to zero at  $r_c$ . For the atoms, we utilize randomly initialized trainable atom type embeddings (Fig. 2a,  $Z_H, Z_C, Z_N$ ). Finally, the bag is represented by the number of remaining atoms (Fig. 2a,  $B$ ).

The action is represented by distances to atoms already placed (Fig. 2a,  $D_Q$ ) as well as a special query type embedding (Fig. 2a,  $Z_Q$ ). When calculating  $Q$ -values the query atom is placed at various voxels allowing for inference of  $Q$ -values at possible positions of the next atom to be placed. In this way, all the encoded distances are easily converted to a 3D structure.

The state representation (Fig. 2b, green) is updated using SchNet-blocks. In the following we will use superscripts to index the blocks, if multiple blocks follow each other. Fully connected layers are given as  $W_i$  where the full details for each fully connected layer is given in the supplementary information. Each block operates on the distance and atom type embeddings using continuous-filter convolutions with skip connections as introduced in SchNet:

$$\tilde{Z}_i^{l+1} = Z_i^l + \sum_{j \neq i} Z_j^l \circ W_d^l(\mathbf{D}_{ij}), \quad (6)$$

where  $\circ$  is elementwise-multiplication and  $Z_i \in \mathbb{R}^d$  are the atom embeddings. The convolution is followed by an atomwise fully connected layer with a skip connection:

$$Z_i^{l+1} = \tilde{Z}_i^{l+1} + W_a^l(\tilde{Z}_i^{l+1}), \quad (7)$$

which is passed to the next SchNet block. By chaining several blocks, information from distant atoms are passed to each atom embedding. After  $L = 5$  layers, the atomwise representations,  $Z_i^L$ , are used for predicting the energy ( $E$ ) of the structure as a combination of local contributions

$$E = \sum_i W_E(Z_i^L) \quad (8)$$

Additionally, we compute a state value ( $SV$ ).

$$SV = W_{SV} \left( W_B(B) \oplus \sum_i Z_i^L \right), \quad (9)$$

where  $\oplus$  is concatenation. The state value is an indication of whether high or low  $Q$ -values are expected from the current state, as will be evident in the next section. Unlike the energy, the state value must consider remaining atoms in the bag when calculating if the current state can progress into a valid molecule.

Having covered the part of the architecture that deals with the state, we now turn to the action part given in Fig. 2b, purple). The query type representation is updated using a single SchNet-block. Furthermore, a multi-head self-attention block over all the atom representations follows. In contrast to local models where information from distant atoms must propagate through

several blocks, self-attention allows for immediate global information flow. In the case of predicting  $Q$ -values for unfinished structures this is especially relevant, as the model must be aware of possible dangling bonds in one end of a molecule while predicting  $Q$ -values in the other end. For  $h = 8$  heads, we calculate a query, key and value as

$$q_i^l = Q^l(Z_i), \quad k_i^l = K^l(Z_i), \quad v_i^l = V^l(Z_i), \quad (10)$$

where the superscript index the head and  $Q^l, K^l, V^l$  are linear projections to a subspace of size  $d_h = d/h$ , where  $Z_i \in \mathbb{R}^d$ . From this, a dot-product attention score is calculated

$$\alpha_{ij}^l = \frac{\exp(q_i^l \cdot k_j^l / \sqrt{d_h})}{\sum_j \exp(q_i^l \cdot k_j^l / \sqrt{d_h})}, \quad (11)$$

which indicates the importance of latent representation  $v_j^l$  to describe  $v_i^l$ . From these scores a new latent representation of  $Z_Q$  is created as

$$Z_Q^l = \sum_j \alpha_{Qj}^l v_j^l \quad (12)$$

which is finally concatenated and processed by a fully connected layer with a skip connection and layer normalization<sup>42</sup>

$$\tilde{Z}_Q = \text{Layer-norm}[Z_Q + W_c(Z_Q^1 \oplus \dots \oplus Z_Q^h)] \quad (13)$$

The representation of the query atom is then used for calculating the  $Q$ -value

$$A = W_A(\tilde{Z}_Q) \quad (14)$$

$$Q = \text{Softmax}(SV + A), \quad (15)$$

where  $A \in \mathbb{R}^{M+1}$ ,  $M$  is the number of atom types, and  $SV \in \mathbb{R}$  is added to the first  $M$  entries of  $A$ . Entry  $i$  in  $Q$  specify the  $Q$ -value for atom type  $i$  and the  $M + 1$ 'th entry allows for low  $Q$ -values for all atom types.  $SV$  enables the network to lower the  $Q$ -value for all possible actions in a given state, instead of independently learning that all actions leads to high-energy structures. By evaluating the  $Q$ -value at multiple voxels, the agent follows the greedy policy of picking the action with the highest  $Q$ -value, leading to the structure in Fig. 2c.

#### IV. METHOD

The algorithm consists of two phases. In the first phase we use a simple form of imitation learning (IL) called behavioral cloning, where the agent learns to build the structures in the database as well as predicting their energies and forces. This agent serves as a starting point for all agents employed in the next phase. In the second phase, a RL process is started where

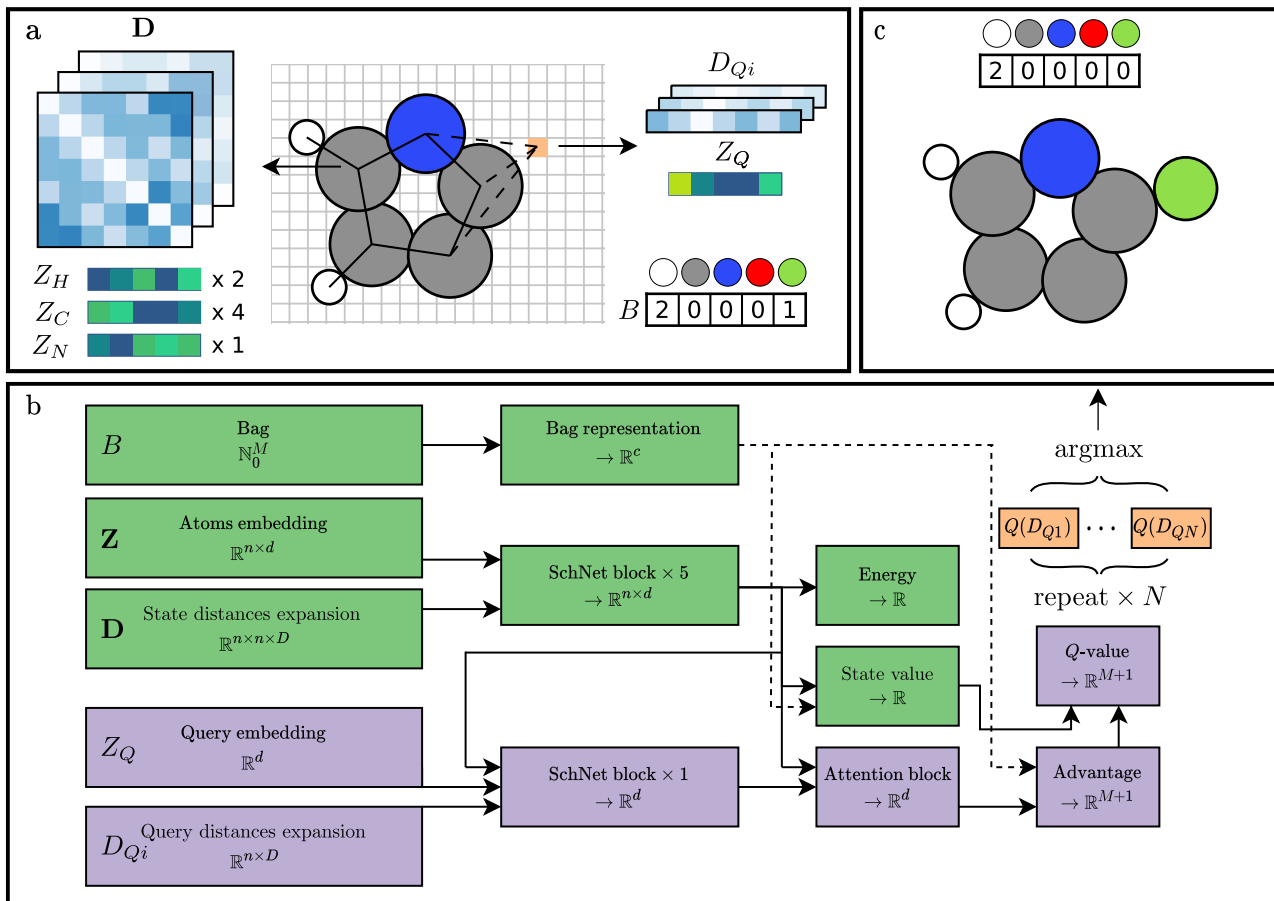


FIG. 2. (a) The molecule is represented as a distance matrix  $D$  (solid lines between atoms) in a Gaussian basis, embeddings for each atom type ( $Z_H, Z_C, Z_N$ ) and a bag  $B$ . An action constitutes an atom placed in one of the voxels. Each action is represented as a distance to the atoms in the state  $D_Q$  (dashed lines, not all distances shown) and a query embedding  $Z_Q$ . (b) To predict  $Q(s, a)$  the network takes as input the state and action representation. The green part of the network operates on the state and the purple section includes the action. The action part is repeated for each voxel in the state resulting in  $N$  possible actions. (c) The resulting state after the voxel with the highest  $Q$ -value is chosen. If the state is terminal the structure is relaxed using the model potential.

stoichiometric-specific agents refines the IL model by constructing new molecules and querying an energy calculator. Based on the received energies and forces, the model updates the  $Q$ -values, energies and forces before constructing a new molecule. As the agents receive feedback from the energy calculator the molecules continue to improve.

### A. Imitation learning phase

To create an initial model the GDB-11 database consisting of molecules containing up to 11 heavy atoms (C,N,O,F) is utilized. Specifically, we use all 1850 structures with 6 heavy atoms for supervised pretraining. Using RDKit<sup>43</sup> SMILES are transformed into 3D structures and a single point density functional theory (DFT) calculation of the energy and forces is performed using GPAW<sup>44,45</sup> using a localized atomic basis set<sup>46</sup>. The

model is then trained using the following loss function

$$l = \rho_E l_E + \rho_F l_F + \rho_Q l_Q, \quad (16)$$

where we have

$$l_E = \|E - \hat{E}\|^2 \quad (17)$$

$$l_F = \frac{1}{3N} \sum_{i=1}^{3N} \text{Huber}(F_i, \hat{F}_i) \quad (18)$$

$$l_Q = - \sum_{i=1}^{M+1} p_i \log \hat{Q}_i, \quad (19)$$

where the hat denotes values predicted by the network and  $\rho_E = 0.1$ ,  $\rho_F = 0.9$  and  $\rho_Q = 1$  are empirically chosen to balance the contributions to the total loss.  $N$  is the number of atoms in the structure, with  $M$  different atom types.

The energy (eq. 17) is trained using a mean squared error (MSE) loss while forces (eq. 18) are updated using a Huber loss given by

$$\text{Huber}(F, \hat{F}) = \begin{cases} \frac{1}{2}(F - \hat{F})^2, & \text{if } |F - \hat{F}| < 1 \\ |F - \hat{F}| - \frac{1}{2}, & \text{else} \end{cases} \quad (20)$$

i.e. a squared loss for small differences and a linear loss for large errors. The Huber loss was more stable by suppressing the effect of large force outliers which were occasionally present in the structures built by the model. Similarly, a cross entropy loss for the  $Q$ -values (eq. 19) was found to be more stable than a MSE for the pretraining phase where only  $Q$ -values of 0 or 1 are required. For the cross entropy loss  $\hat{Q}_i$  refers to the  $Q$ -value for atom type  $i$  and we set  $p_i = 1$  for the atom type placed in the database and 0 for the other types. Additionally, for each action present in the database we generate five perturbed actions by randomly moving the selected atom and setting  $p_i = 1$  for the  $M + 1$ 'th entry in the  $Q$ -value prediction, thereby enforcing  $Q$ -values for all atom types to be zero for the randomly generated actions. As this generates an imbalance in the training data the valid actions are weighted by a factor of five.

The model is implemented in Pytorch<sup>47</sup> and trained using the Adam<sup>48</sup> optimizer with an initial learning rate of  $5 \cdot 10^{-3}$  and a batch size of 384. We use 90% of the structures for training the remaining 10% are used as a validation set for decaying the learning rate by a factor of 2 when the validation error plateaus for 30 epochs. Once the learning rate decayed below  $10^{-6}$  the validation loss stagnated, and the final model is chosen for employment in the RL phase.

## B. Reinforcement learning phase

In the RL phase we deploy the IL model for all 135 stoichiometries present in the training set. A cubic cell of dimension [20Å, 20Å, 20Å] and a  $Q$ -value grid resolution of 0.2Å is chosen, with the initial atom restricted to the center of the cell. We use a modified  $\varepsilon$ -greedy strategy, to trade-off exploration and exploitation. To satisfy two random moves per episode in expectation, we choose a greedy action with probability  $1-2/T$  and a random action with probability  $2/T$ , where  $T$  is the number of atoms in the structure. We choose 5% of random actions uniformly random, while the other 95% are uniformly sampled from the top 5% of actions. Furthermore, all hydrogen atoms are masked until all other atom types are placed which reduces the action space without excluding any molecules. Due to the IL model an action among the highest  $Q$ -values is frequently taken which ensures exploration while simultaneously suppressing the large fraction of actions resulting in completely invalid molecules. To limit the action space, we only allow actions which fulfill

$$c_1[r_{\text{cov}}(a) + r_{\text{cov}}(i)] < r_{ai} < c_2[r_{\text{cov}}(a) + r_{\text{cov}}(i)], \quad (21)$$

for at least one atom  $i$  already present in the structure. Here  $c_1 = 0.75$ ,  $c_2 = 1.25$  and  $r_{\text{cov}}(i)$  is the covalent radius of atom  $i$ .  $r_{\text{cov}}(a)$  is the covalent radius of the atom placed in action  $a$  and  $r_{ai}$  is the distance between the new atom and a present atom  $i$ . That is, the new atom must be placed within 0.75 to 1.25 times the sum of the covalent radii of itself and an already present atom. This restricts the model to building non-fragmented structures for a better comparison with the database.

The agent trained as detailed in the previous section is perfectly capable of building a variety of different molecules given a predetermined stoichiometry. Owing to the stochastic nature of the modified  $\varepsilon$ -greedy policy employed sequential builds using the same agent results in different structures being built.

We exploit that to construct a first ensemble of structures by tasking the agent with building molecules 200 times. It does so according to the pretrained  $Q$ -values and every completed structure is subject to a relaxation in the model energy, eq. (8), followed by snapping the molecule back on the grid. If the relaxation results in a fragmentation of the molecule into several pieces, the original structure is used instead. The initial exploration phase promotes exploration of a large part of configuration space to avoid premature convergence to a local minimum. Since the model is pretrained the generated molecules will generally be of high quality.

Once the first 200 builds are completed, the search enters the RL mode. Here the algorithm alternates between generating a structure and updating the model using five mini-batches until a total of 600 additional molecules have been generated. For the  $Q$ -values the loss function is changed to MSE, since the target is now given by eq. (2), i.e. it is no longer 0 or 1, but depends on the potential energy of the molecule. By further improving the  $Q$ -values and force-predictions the search is directed towards low-energy regions of configuration space.

## C. GDB-11 benchmark

We start by testing the performance of the current framework when it comes to identifying molecules with stoichiometries already present in the database used for the training. The search is conducted as a set of 64 independent restarts following the outlined protocol: using the data-based-trained agent for 200 builds and applying RL for 600 subsequent builds. To facilitate the quantification of the amount of new structures found, we resort to the use of SMILES, as an analytic tool. We stress that SMILES are not used in any way by the agents as this would limit the scope of these. Once the search is finished all structures are post processed by taking five gradient steps using the *final* energy landscape. This is a computationally cheap step that removes uncertainties from the original relaxation of the molecules in the less reliable model energy landscape that had been learned up to the point of the RL generating the particular molecule

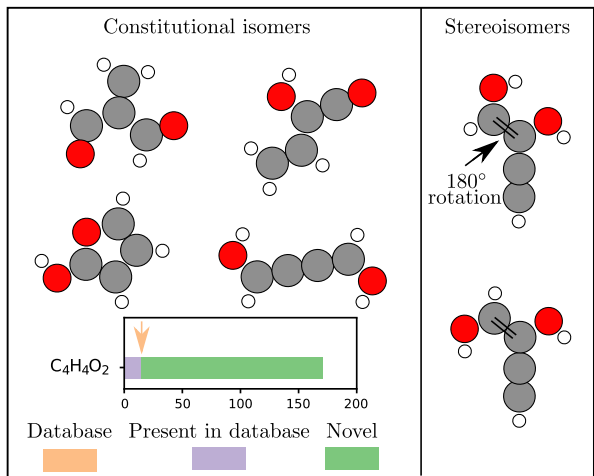


FIG. 3. Subset of discovered constitutional isomers (left) and stereoisomers (right) for  $C_4H_4O_2$ . Further shown is the number of all unique constitutional isomers in the database (orange arrow) as well as the molecules produced by ASLA divided into molecules present in the database (purple bar) and novel molecules (green bar).

as well as unfortunate grid snapping. These re-relaxed structures are then converted to SMILES and all unique constitutional isomers are found. To this end, we show in Fig. 3 some of the molecules being built when searching for  $C_4H_4O_2$ . As illustrated, we find both new constitutional isomers and often several stereoisomers for these. Looking across these 64 restarts, all of the structures of this composition present in the database (orange arrow) are found again (purple bar). However, also a considerable number of molecules not present in the database are found (green bar).

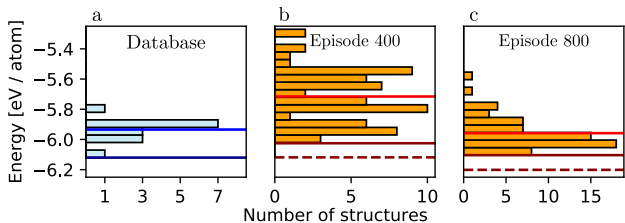


FIG. 4. DFT energy distribution of the molecules. (a) Molecules in the database. Blue line is the average energy and dark blue line is the lowest energy isomer. (b) Orange: structures built in episode 400. The red line indicates the mean energy of the structure and the dark red shows the mean of the lowest energy structure in each run found before episode 400. Finally, the dark red dashed line shows the lowest energy isomer among the 64 parallel runs, found before episode 400. (c) Same as (b), but now at 800 episodes. As the search progresses a shift towards lower energies is observed.

To investigate whether the produced molecules are of low energy we illustrate the evolution of the 64 agents from episode 400 to 800 in Fig. 4. The histograms indicate the energy distribution of the structures built in

the given episode across the 64 agents. As the search progresses the distribution shifts towards lower energies as the model begins converging, which is further evident by the mean of the distribution (red line) shifting down. Similarly, when we only consider the mean of the lowest energy structure in each run (i.e. not necessarily built in episode 400 or 800), which is depicted using dark red we see a similar shift. In blue, the average energy of the structures in the database, snapped to the grid ASLA operates on, is given. Initially the database is better than the average built of the agent due to imperfect fitting to the database but is overtaken by the agent at episode 800. If one looks only at the best structure in the database (dark blue) the average lowest energy approaches this limit and is marginally beaten by one of the isomers (dark red, dashed). Fully relaxing all unique isomers in DFT indeed reveals that the lowest energy isomer produced by ASLA coincides with the minimum structure in the database.

To observe the decision process for the RL algorithm we plot the  $Q$ -values for one of the runs in figure 5. First of all, the model has clearly learned a great deal about chemical bonding and thus generally suppresses invalid actions, predicting only high  $Q$ -values for sensible bonding sites. The agent is fully aware of possible symmetries during the build. Starting with a single atom in  $s_1$ , the  $Q$ -values have spherical symmetry. For the linear dimer in  $s_2$  the symmetry of the  $Q$ -values reduces to a ring, and for the Y-shaped  $C_3O$  backbone in  $s_5$ , two symmetric 'caps' of high  $Q$ -values develop. As evident in states  $s_4$ - $s_8$  where multiple sites have high  $Q$ -values, the model decides between different possible isomers when building the molecule. Bond lengths chosen early on e.g. the C-C bond lengths when placing the C atoms from  $s_2$  to  $s_5$  have an impact on later  $Q$ -values. The  $Q$ -values encircled by a black ellipse in  $s_8$  are thus smaller than the  $Q$ -value that are chosen upon building  $s_9$ . In both cases, aldehyde (HOC-) groups are formed, but at C atoms involved in double or single C-C bonds, respectively, the latter being the energetically preferred. Placing H atoms at both sites would have been possible causing tautomerization involving the methyl group, but again given the initial choices for C-C bond lengths, this is no longer preferable as reflected by the  $Q$ -values in  $s_9$ . Owing to the modified  $\epsilon$ -greedy policy, such alternative molecular builds are occasionally made despite the C-C bond lengths, and the subsequent relaxation in the on-the-fly learned model will provide properly adjusted molecules for the RL training.

In Fig. 6 the total number of structures found after 800 episodes for the 15 stoichiometries with most isomers in the database are shown. For a figure involving all 135 stoichiometries, see supplementary Fig. 1. Similarly to earlier, purple bars indicate the structures present in both the search and the database, whereas green indicate novel structures. A majority of the structures in the database (orange line) are found within the 800 episodes

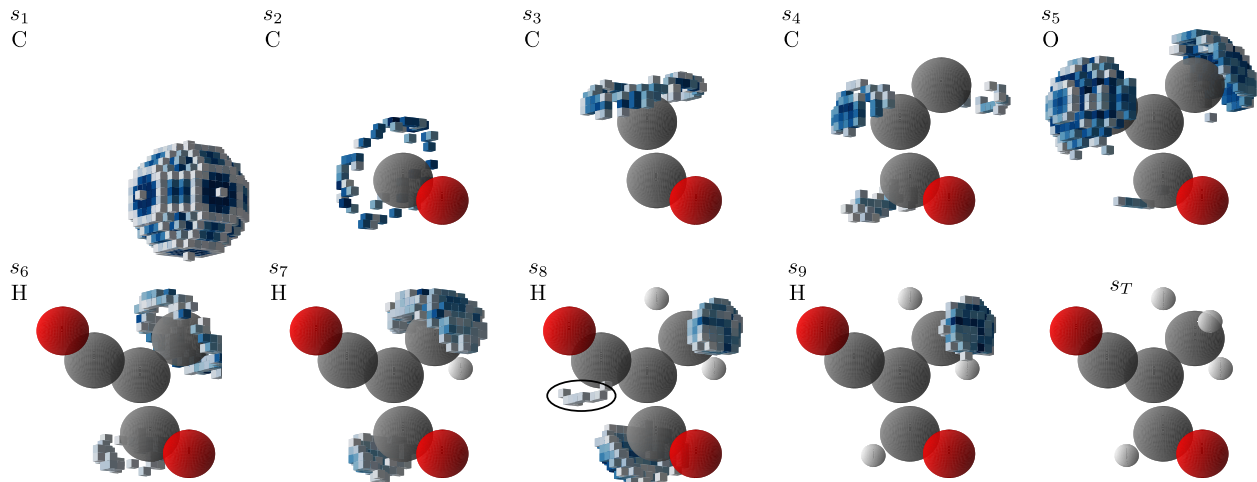


FIG. 5. All  $Q$ -values above 0.7 are shown with darker blue corresponding to higher  $Q$ -values. For each state we only show the  $Q$ -values corresponding to the atom placed in the given step.

using 64 searches. In total 1769 of the 1850 molecules in the database are found, i.e. slightly more than the 1665 structures used for the training set. Accounting for both novel molecules and structures rediscovered from the database, 20074 unique constitutional isomers are generated resulting in a 10-fold increase of the database. Especially for stoichiometries where multiple bond combinations are possible, i.e. for stoichiometries containing a lot of carbon, oxygen and nitrogen several new constitutional isomers are discovered, whereas for hydrocarbons and  $C_xH_yF_z$  where a lot of single bonds are present the database covers a large fraction of the isomers.

If the RL is neglected and the IL model is used for sampling in all 800 episodes, 1649 of the structures in the database and 15709 novel molecules are generated for a total of 17358 unique constitutional isomers. The IL model thus covers a large fraction of the produced structures and turning on RL provides 15.6% more molecules.

To illustrate the difference between the IL model and the RL version, we plot the average atomization energy per atom of the structures generated by ASLA throughout the 800 episodes (fig. 7) and compare it to the energies of the structures in the database when placed on the same  $0.2\text{\AA}$  resolution grid. For each ASLA curve the average is over the 64 independents run as earlier and now also the 135 stoichiometries. As previously observed, the model trained on the database starts out by producing higher energy structures (red curve) than the average structure in the database (blue curve), due to the imperfect fitting of the database. Similarly, the average of the best structures (dark red) is worse than the lowest energy isomer in the database (dark blue). At around 500 episodes both the average and best structures produced by ASLA marginally outperforms the database. At 800 episodes the best structure is outperformed by

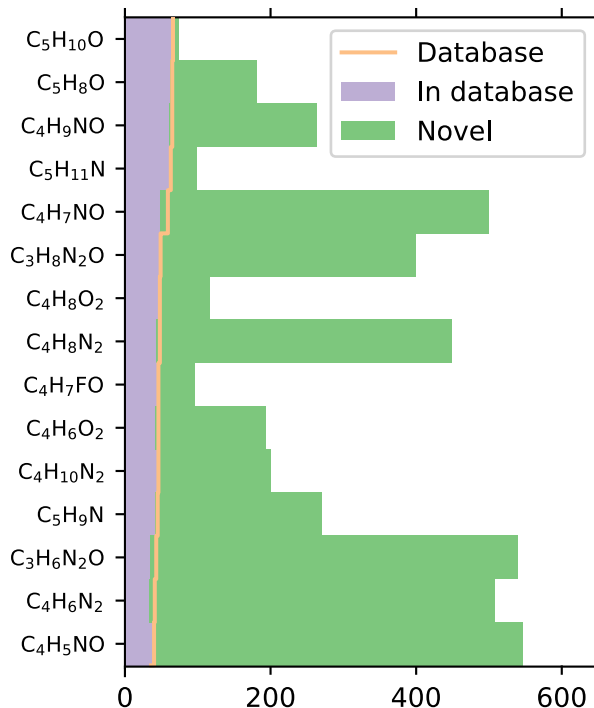


FIG. 6. Molecules discovered. Orange line: number of constitutional isomers in the database. Purple bars: molecules found that are also present in the database. Green bars: novel molecules found.

$0.04\text{ eV/atom}$  on average. If one only looks at the best structure in each of the 64 runs (dark red, dashed) the database is outperformed by  $0.09\text{ eV/atom}$ .

In order to check if this energy difference amounts to new low energy structures the specific *stereoisomers* in the database and the structures generated by ASLA are compared. In that case 1742 of the molecules in the

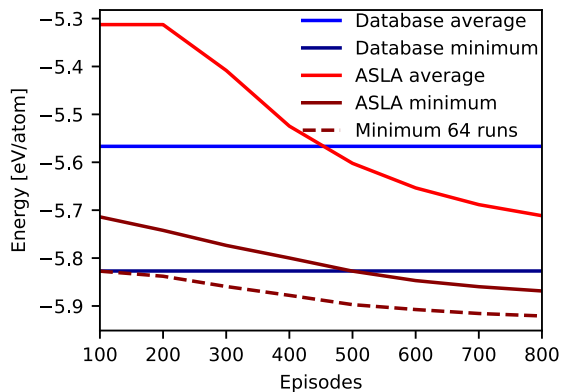


FIG. 7. Blue: average energy of structures in the database. Dark blue: average energy of lowest energy molecules in the database. Red: average energy of structures built by ASLA. Dark red: average energy of lowest energy molecules found by ASLA. Dashed dark red: lowest energy isomer among the 64 runs.

database are found. When counting *constitutional* isomers as in Fig. 6, 1769 of the structures in the database were found, which means that in 27 cases the stereoisomer in the database is not found, but the constitutional isomer is. In total, 29049 stereoisomers not present in the database and generated by ASLA is then fully relaxed using DFT, which shows that for each stoichiometry the lowest energy stereoisomer in the database is found by ASLA for all but one stoichiometry and in 72 of 135 stoichiometries a lower energy stereoisomer is found.

#### D. Exploration beyond the database

Having shown that the ASLA framework is capable of reproducing and expanding molecular structures of compositions already present in the database, we now move to explore its performance when applied outside the realms of the database.

As an example, we investigate  $C_9H_8O_4$ , a molecule with twice as many heavy elements as in the training set. As before, 64 independent runs are started.

In Fig. 8a the number of unique constitutional isomers generated as a function of episode number for the IL model (blue) and the model with RL (red) is seen. Unlike for the smaller molecules in IV. C where the IL model was sufficient to cover a large fraction of configuration space there is now a significant difference between the RL and IL agent. The RL model clearly outperforms the IL model in terms of number of molecules generated as the search progresses, showing that the on-the-fly training is able to correct inefficiencies in the initial version. However, the ultimate goal is to generate low energy molecules. Hence, in Fig. 8b the atomization-energy-density of the generated molecules for both the IL

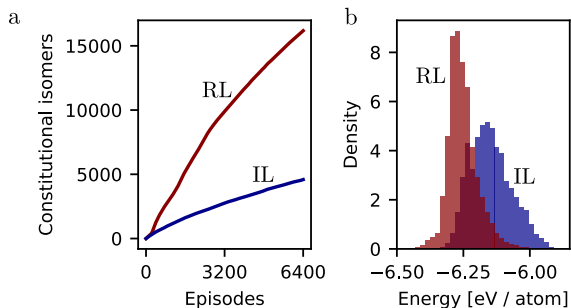


FIG. 8. Searching for  $C_9H_8O_4$  isomers. (a) Constitutional isomers found as the search progresses. As the search progresses the RL version (red) quickly produces more structures than the IL version. (b) Energy-density of the generated structures. In addition to producing more structures, the RL version (red) generates a larger fraction of low energy molecules.

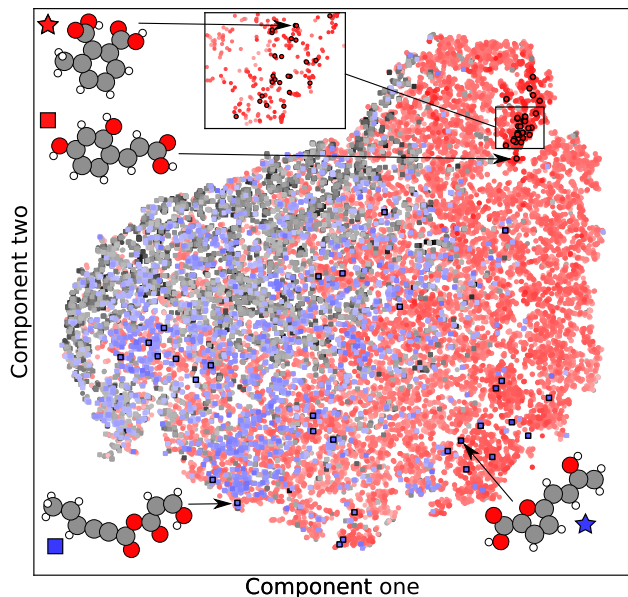


FIG. 9. Searching for  $C_9H_8O_4$  isomers. 2D visualization of IL agent (squares) and RL version (circles). All structures are colored by their energy on a scale from grey to blue (IL) or red (RL). The 30 lowest energy structures for both versions of the algorithms are framed in black.

model and the RL version is seen. As before all stereoisomers are fully relaxed using DFT. The molecules generated by the RL-enhanced model are significantly more stable than the IL model, with an average energy difference of 0.105 eV/atom or 2.22 eV per structure. Thus, the RL version does not only cover more of configuration space, it is also able to focus on the low energy regions. In Fig. 9 we investigate a 2D visualization of the generated molecules for both the IL model (squares colored grey to blue) and RL version (circles colored grey to red). The structures are represented using smooth overlap of atomic positions<sup>49</sup> (SOAP) in a 2D space using t-SNE and colored by their energy using two different



color schemes to help guide the eye. The 30 lowest energy structures found for both models are framed in black and can be seen in the supplementary. The RL version discovers certain low energy regions such as compact aromatic molecules as shown in the inset. The IL version, however, is not able to extrapolate into this region based on what it has learned from the database. Interesting molecules among the low energy isomers include the lowest energy isomer found by the search (red star) as well as the second lowest isomer (see supplementary) that both resemble uvitic acid. The search discovers umbellic acid (red square) and caffeic acid (just outside top 30). Additionally, the RL model discovers a stable isomer with a 7-membered ring (supplementary), a substructure not present in the original database as only molecules with up to 6 heavy atoms were used. Despite this, the RL model learns to construct such molecules which would have been hard to discover by a pure supervised generative approach.

For the IL model we observe fewer of the common aromatic molecules as it has no driving force towards low energy regions of configuration space, as exemplified by the lowest energy isomer found (blue star) being 2 eV higher in energy than the corresponding lowest energy structure in the RL version. The missing focus on low energy parts of configuration space results in the 30 lowest energy structures being scattered across the 2D space, mostly composed of elongated structures (such as the blue square) where subparts, unlike large aromatic rings, are more dominant in the GDB-11 database. Utilizing the feedback from the RL is thus crucial to correct flaws in the IL model as well as expanding beyond knowledge in the database.

## V. CONCLUSION

We have presented a framework for autonomous construction of molecules. The method relies on a pre-existing database which via supervised learning provides a base level for a model used for constructing new molecules. Further training of the model is done in a reinforcement learning setting where feedback is provided by single point energy calculations by a high-level quantum mechanical total energy method. The resulting model is able to reproduce structures in the database as well as producing novel structures. The introduced model is able to operate directly in 3D space allowing for biasing the search towards stable molecules. When applying the imitation learning model in domains far from the training set, the reinforcement learning procedure corrects initial shortcomings in the model. Further work in this direction could investigate building molecules in specific environments, such as organic light-emitting diode (OLED) or organic solar panels where properties such as HOMO-LUMO gap could be included in the reward function together with the stability.

## VI. ACKNOWLEDGMENTS

We acknowledge support from VILLUM FONDEN (Investigator grant, Project No. 16562). This work has been supported by the Danish National Research Foundation through the Center of Excellence "InterCat" (Grant agreement no.: DNRF150)

## VII. REFERENCES

- B. Hartke, *The Journal of Physical Chemistry* **97**, 9973 (1993).
- J. H. J. Emilie S. Henault, Maria H. Rasmussen, *PeerJ Physical Chemistry* **2** (2020), 10.7717/peerj-pchem.11.
- D. J. Wales and J. P. K. Doye, *The Journal of Physical Chemistry A* **101**, 5111 (1997).
- J. Kennedy and R. Eberhart, in *Proceedings of ICNN'95 - International Conference on Neural Networks*, Vol. 4 (1995) pp. 1942–1948 vol.4.
- E. L. Kolsbjerg, A. A. Peterson, and B. Hammer, *Phys. Rev. B* **97**, 195424 (2018).
- S. A. Meldgaard, E. L. Kolsbjerg, and B. Hammer, *The Journal of Chemical Physics* **149**, 134104 (2018).
- R. Winter, F. Montanari, A. Steffen, H. Briem, F. Noé, and D.-A. Clevert, *Chem. Sci.* **10**, 8016 (2019).
- E. K. B. James L. Melville and J. D. Hirst, *Combinatorial Chemistry and High Throughput Screening* **12**, 332 (2009).
- K. A. Carpenter and X. Huang, *Current Pharmaceutical Design* **24**, 3347 (2018).
- J. J. Irwin and B. K. Shoichet, *Journal of Chemical Information and Modeling* **45** (2005), 10.1021/ci049714+.
- L. Ruddigkeit, R. van Deursen, L. C. Blum, and J.-L. Reymond, *Journal of Chemical Information and Modeling* **52** (2012), 10.1021/ci300415d.
- R. Ramakrishnan, P. O. Dral, M. Rupp, and O. A. von Lilienfeld, *Scientific Data* **1** (2014), 10.1038/sdata.2014.22.
- S. Haastrup, M. Strange, M. Pandey, T. Deilmann, P. S. Schmidt, N. F. Hinsche, M. N. Gjerding, D. Torelli, P. M. Larsen, A. C. Riis-Jensen, J. Gath, K. W. Jacobsen, J. J. Mortensen, T. Olsen, and K. S. Thygesen, *2D Materials* **5**, 042002 (2018).
- K. T. Winther, M. J. Hoffmann, J. R. Boes, O. Mamun, M. Bajdich, and T. Bligaard, *Scientific Data* **6**, 75 (2019).
- Y. Li, L. Zhang, and Z. Liu, "Multi-objective de novo drug design with conditional graph generative model," (2018), arXiv:1801.07299.
- A. Gupta, A. T. Müller, B. J. H. Huisman, J. A. Fuchs, P. Schneider, and G. Schneider, *Molecular Informatics* **37**, 1700111 (2018).
- R. Gómez-Bombarelli, J. N. Wei, D. Duvenaud, J. M. Hernández-Lobato, B. Sánchez-Lengeling, D. Sheberla, J. Aguilera-Iparraguirre, T. D. Hirzel, R. P. Adams, and A. Aspuru-Guzik, *ACS Central Science* **4**, 268 (2018).
- A. Zhavoronkov, Y. A. Ivanenkov, A. Aliper, M. S. Veselov, V. A. Aladinskiy, A. V. Aladinskaya, V. A. Terentiev, D. A. Polykovskiy, M. D. Kuznetsov, A. Asadulaev, Y. Volkov, A. Zhulus, R. R. Shayakhmetov, A. Zhebrak, L. I. Minaeva, B. A. Zagribelnyy, L. H. Lee, R. Soll, D. Madge, L. Xing, T. Guo, and A. Aspuru-Guzik, *Nature Biotechnology* **37**, 1038 (2019).
- F. Noé, S. Olsson, J. Köhler, and H. Wu, *Science* **365**, eaaw1147 (2019).
- M. Hoffmann and F. Noé, "Generating valid euclidean distance matrices," (2019), arXiv:1910.03131.
- N. W. A. Gebauer, M. Gastegger, and K. T. Schütt, "Symmetry-adapted generation of 3d point sets for the targeted discovery of molecules," (2019), arXiv:1906.00957.
- E. Mansimov, O. Mahmood, S. Kang, and K. Cho, *Scientific Reports* **9**, 20381 (2019).

- <sup>23</sup>L. Maziarka, A. Pocha, J. Kaczmarczyk, K. Rataj, T. Danel, and M. Warchol, *Journal of Cheminformatics* **12**, 2 (2020).
- <sup>24</sup>J. Köhler, L. Klein, and F. Noe, in *Proceedings of the 37th International Conference on Machine Learning*, Proceedings of Machine Learning Research, Vol. 119, edited by H. D. III and A. Singh (PMLR, 2020) pp. 5361–5370.
- <sup>25</sup>V. G. Satorras, E. Hoogeboom, F. B. Fuchs, I. Posner, and M. Welling, “E(n) equivariant normalizing flows for molecule generation in 3d,” (2021), arXiv:2105.09016.
- <sup>26</sup>R. Winter, F. Noé, and D.-A. Clevert, “Permutation-invariant variational autoencoder for graph-level representation learning,” (2021), arXiv:2104.09856.
- <sup>27</sup>M. Olivecrona, T. Blaschke, O. Engkvist, and H. Chen, *Journal of Cheminformatics* **9**, 48 (2017).
- <sup>28</sup>E. Putin, A. Asadulaev, Y. Ivanenkov, V. Aladinskiy, B. Sanchez-Lengeling, A. Aspuru-Guzik, and A. Zhavoronkov, *Journal of Chemical Information and Modeling* **58**, 1194 (2018).
- <sup>29</sup>N. D. Cao and T. Kipf, “Molgan: An implicit generative model for small molecular graphs,” (2018), arXiv:1805.11973.
- <sup>30</sup>M. Popova, O. Isayev, and A. Tropsha, *Science Advances* **4**, eaap7885 (2018).
- <sup>31</sup>Z. Zhou, S. Kearnes, L. Li, R. N. Zare, and P. Riley, *Scientific Reports* **9**, 10752 (2019).
- <sup>32</sup>J. S. Schreck, C. W. Coley, and K. J. M. Bishop, *ACS Central Science* **5**, 970 (2019).
- <sup>33</sup>G. Simm, R. Pinsler, and J. M. Hernandez-Lobato, in *Proceedings of the 37th International Conference on Machine Learning*, Proceedings of Machine Learning Research, Vol. 119, edited by H. D. III and A. Singh (PMLR, 2020) pp. 8959–8969.
- <sup>34</sup>M. S. Jørgensen, H. L. Mortensen, S. A. Meldgaard, E. L. Kolsbjerg, T. L. Jacobsen, K. H. Sørensen, and B. Hammer, *The Journal of Chemical Physics* **151**, 054111 (2019).
- <sup>35</sup>T. Fink, H. Bruggesser, and J.-L. Reymond, *Angewandte Chemie International Edition* **44**, 1504 (2005).
- <sup>36</sup>W. Gao and C. W. Coley, *Journal of Chemical Information and Modeling* **60**, 5714 (2020), <https://doi.org/10.1021/acs.jcim.0c00174>.
- <sup>37</sup>D. Weininger, *Journal of Chemical Information and Computer Sciences* **28**, 31 (1988).
- <sup>38</sup>H. L. Mortensen, S. A. Meldgaard, M. K. Bisbo, M.-P. V. Christiansen, and B. Hammer, *Phys. Rev. B* **102**, 075427 (2020).
- <sup>39</sup>K. T. Schütt, H. E. Sauceda, P. Kindermans, A. Tkatchenko, and K. Müller, *The Journal of Chemical Physics* **148**, 241722 (2018).
- <sup>40</sup>A. Vaswani, N. Shazeer, N. Parmar, J. Uszkoreit, L. Jones, A. N. Gomez, L. u. Kaiser, and I. Polosukhin, in *Advances in Neural Information Processing Systems*, Vol. 30, edited by I. Guyon, U. V. Luxburg, S. Bengio, H. Wallach, R. Fergus, S. Vishwanathan, and R. Garnett (Curran Associates, Inc., 2017).
- <sup>41</sup>M. Machado, M. Bellemare, E. Talvitie, J. Veness, M. Hausknecht, and M. Bowling, *Journal of Artificial Intelligence Research* , 5573 (2018).
- <sup>42</sup>J. L. Ba, J. R. Kiros, and G. E. Hinton, “Layer normalization,” (2016), arXiv:1607.06450.
- <sup>43</sup>G. Landrum, “Rdkit: Open-source cheminformatics; <http://www.rdkit.org>,”.
- <sup>44</sup>J. J. Mortensen, L. B. Hansen, and K. W. Jacobsen, *Phys. Rev. B* **71**, 035109 (2005).
- <sup>45</sup>J. Enkovaara, C. Rostgaard, J. J. Mortensen, J. Chen, M. Dulak, L. Ferrighi, J. Gavnholt, C. Glinsvad, V. Haikola, H. A. Hansen, H. H. Kristoffersen, M. Kuisma, A. H. Larsen, L. Lehtovaara, M. Ljungberg, O. Lopez-Acevedo, P. G. Moses, J. Ojanen, T. Olsen, V. Petzold, N. A. Romero, J. Stausholm-Møller, M. Strange, G. A. Tritsarlis, M. Vanin, M. Walter, B. Hammer, H. Häkkinen, G. K. H. Madsen, R. M. Nieminen, J. K. Nørskov, M. Puska, T. T. Rantala, J. Schiøtz, K. S. Thygesen, and K. W. Jacobsen, *Journal of Physics: Condensed Matter* **22**, 253202 (2010).
- <sup>46</sup>A. H. Larsen, M. Vanin, J. J. Mortensen, K. S. Thygesen, and K. W. Jacobsen, *Phys. Rev. B* **80**, 195112 (2009).
- <sup>47</sup>A. Paszke, S. Gross, F. Massa, A. Lerer, J. Bradbury, G. Chanan, T. Killeen, Z. Lin, N. Gimelshein, L. Antiga, A. Desmaison, A. Köpf, E. Yang, Z. DeVito, M. Raison, A. Tejani, S. Chilamkurthy, B. Steiner, L. Fang, J. Bai, and S. Chintala, “Pytorch: An imperative style, high-performance deep learning library,” (2019), arXiv:1912.01703.
- <sup>48</sup>D. P. Kingma and J. Ba, “Adam: A method for stochastic optimization,” (2014), 1412.6980.
- <sup>49</sup>A. P. Bartók, R. Kondor, and G. Csányi, *Phys. Rev. B* **87**, 184115 (2013).

VIII. SUPPLEMENTARY

A. Network details

In table. I a detailed overview of the blocks in the network is given. The activation function is a shifted softplus<sup>39</sup> (ssp) given by

$$\text{ssp}(x) = \ln(0.5e^x + 0.5) \tag{22}$$

Bag representation	$W_B$	(5, 16, spp, 32)
Atomwise layers	$W_a$	(64, 64, spp)
Distances representation	$W_d$	(20, 64, spp)
State Value	$W_{SA}$	(96, 32, spp, 1)
Advantage	$W_A$	(96, 32, spp, 6)
Energy	$W_E$	(64, 32, spp, 16, spp, 8, spp, 1)
Concatenation layer	$W_c$	(64, 64)

TABLE I. Dimension of data as it passes through the fully connected layers. The activation function is is the shifted softplus indicated by spp.



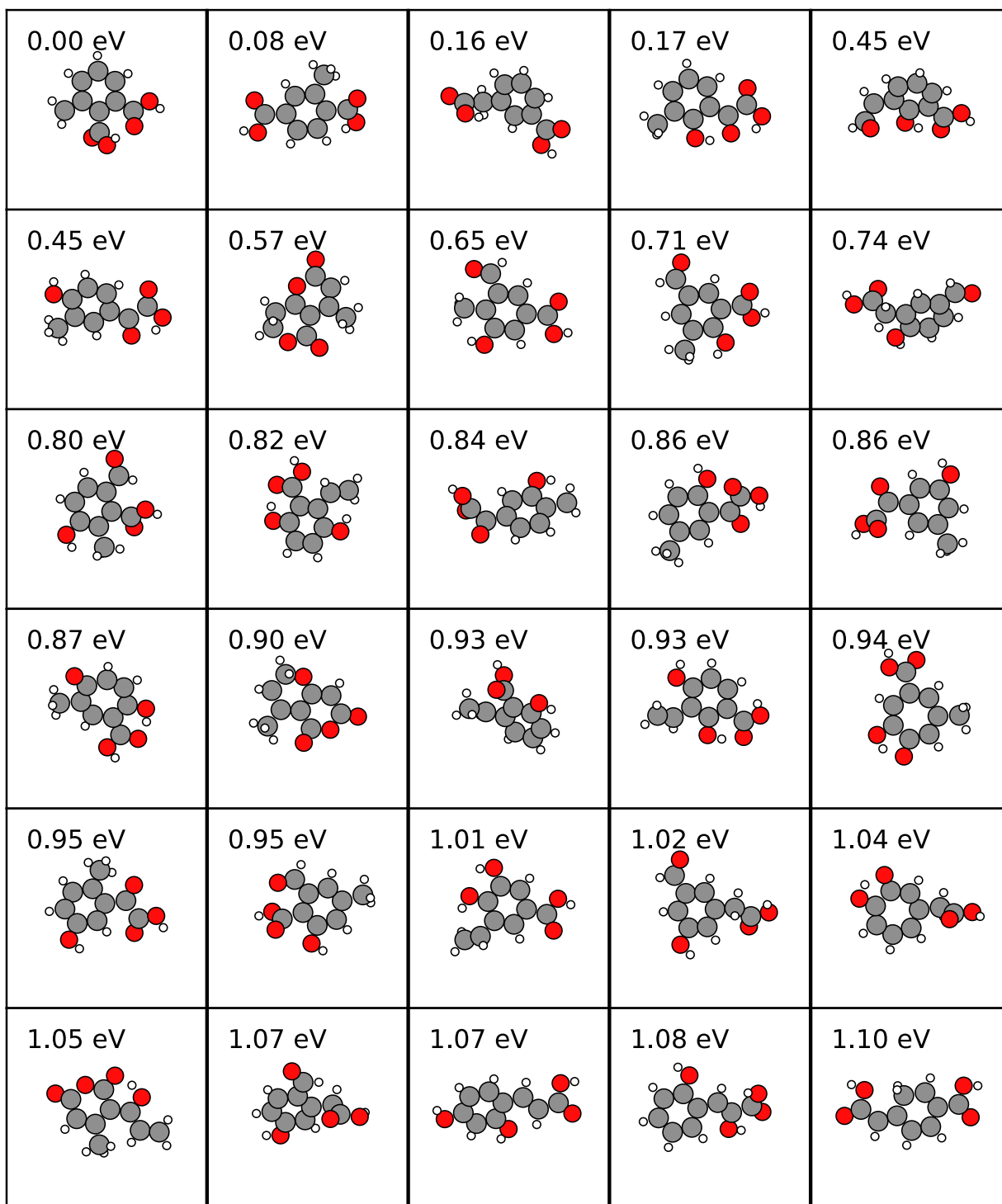


FIG. 2. 30 lowest energy structures for the RL run.

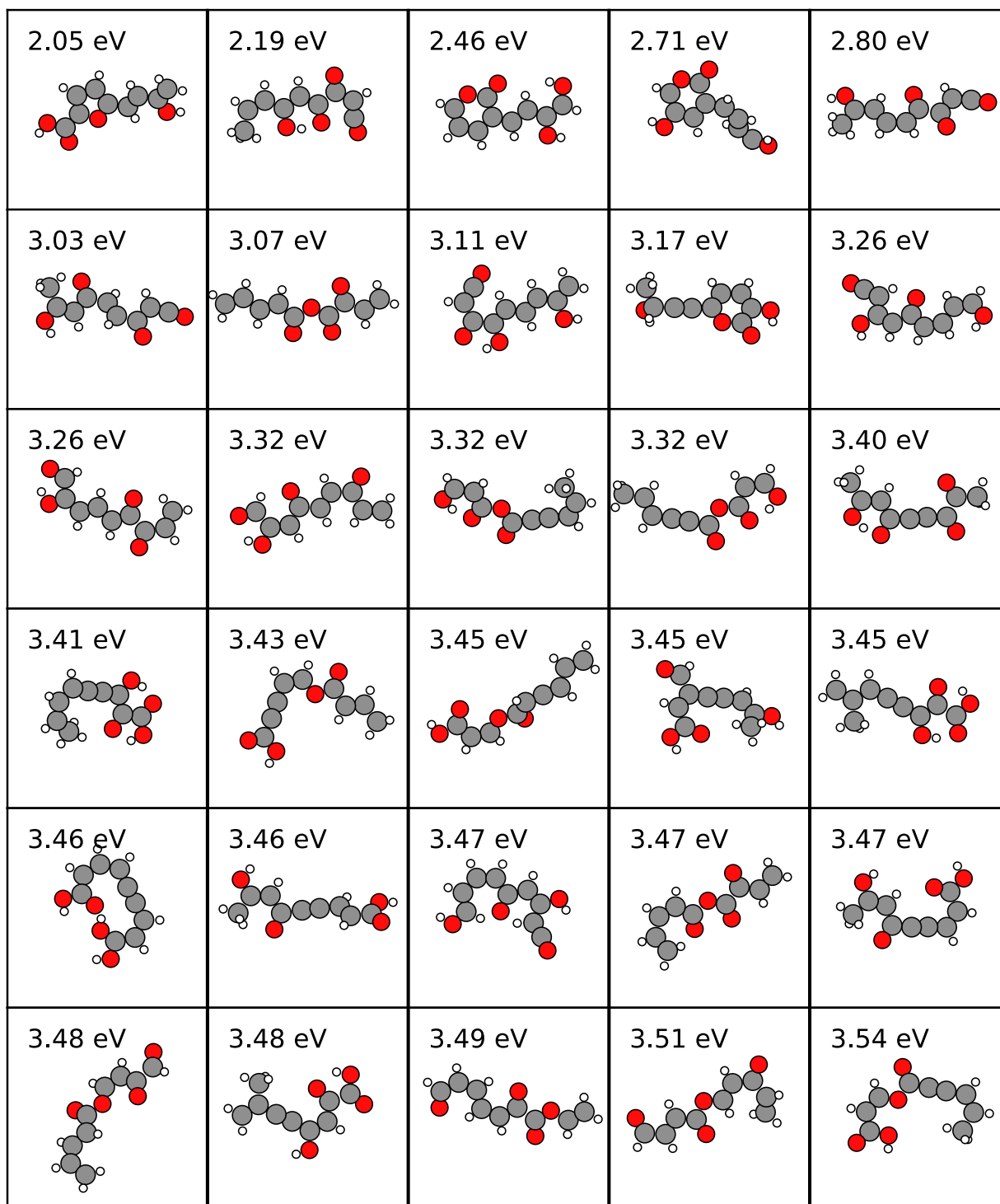


FIG. 3. 30 lowest energy structures for the IL run. Energies are relative to the lowest energy isomer found in the RL version.